Eur. J. Mech., B/Fluids, **17**, n° 2, 219-237, 1998

Characterizing boundary-layer instability at finite Reynolds numbers

J. J. HEALEY*

ABSTRACT. – When the Reynolds number is treated as an asymptotically large number in a boundary-layer stability analysis, it is possible to identify Reynolds number scalings at which different terms in the governing equations balance. These balances determine which physical mechanisms are operating under which circumstances and enable a systematic treatment of the various parameter regimes to be carried out. Linear waves can grow by viscous mechanisms if the velocity profile is noninflexional and both viscous and inviscid instabilities are present for inflexional profiles. When disturbances become nonlinear the resulting dynamics depend upon the type of instability and, in particular, on whether the critical layer lies within the viscous wall layer or is separate from it. Therefore, the classification of a wave as viscous or inviscid is important to the theory of transition.

However, at finite Reynolds numbers the boundaries separating different types of instability become blurred. Moreover, certain asymptotic theories are known to give poor quantitative agreement with experiment while others remain untested by detailed experimental comparison. This paper is concerned with identifying the domains where the different asymptotic theories are most relevant so as to facilitate their comparison with experiment. Numerical solutions of the Orr-Sommerfeld equation are presented that indicate that in wind-tunnel experiments the instability driving transition is esssentially viscous even for adverse pressure gradient boundary layers, and that inviscid instability waves would be difficult to observe. For an inviscid wave near the upper branch there could be a lower frequency viscous wave at the same point in the flow with amplitude 50 times larger in a typical practical situation. © Elsevier, Paris.

1. Introduction

Transition to turbulence in a boundary layer is a nonlinear process, but the way in which nonlinearity develops depends on the linear behaviour of initially small disturbances. This is especially true when using the method of matched asymptotic expansions to construct theories for the disturbance's evolution. The first step then, towards understanding, predicting and perhaps controlling transition, is to establish which linear amplification mechanisms are operating under given conditions.

There are many circumstances when making the parallel flow approximation for small disturbances in a boundary-layer flow gives acceptably accurate predictions for the growth and decay of those disturbances. The assumption of parallel flow allows distrubances to be treated as a sum of normal modes that are described by the Orr-Sommerfeld equation. However, the parallel flow approximation does not always give good predictions, and is particularly inappropriate close to the leading edge of an aerofoil, which has consequences for swept wings. Moreover, in practice, we are really interested in the nonlinear evolution since this is what causes transition. Direct numerical simulation of the full nonlinear problem remains an unsuitable approach to practical wing-design and so nonlinear theories are an important supplement to, and offer guidance to, experimental work. Weakly nonlinear theories exploit the slow growth of disturbances close to a neutral curve to predict how nonlinearity first modifies the linear growth. However, nonparallel effects are necessarily more important

* Department of Mathematics, Keele University, Staffordshire ST5 5BG, UK.

0997-7546/98/02/© Elsevier, Paris

for these weakly nonlinear theories because the basic flow must now be essentially constant over distances comparable to the length scale of the slow disturbance growth instead of the wavelength of the disturbance required for linear theory.

The parallel flow approximation involves neglecting the role of viscosity in causing the boundary layer to grow downstream while simultaneously including viscosity in the distubance equations so that the nonslip boundary condition at the wall can be satisfied. This is inconsistent because in the derivation of the Orr-Sommerfeld equation, both effects are of the same order. However, at large Reynolds numbers, it turns out that this is a justifiable approach since the wavelengths of unstable waves can be shown to be such that the boundary layer does not grow significantly over these distances. This explains the success of the Orr-Sommerfeld theory at finite, but numerically large, Reynolds numbers. Gaster (1974) has shown how to correct the Orr-Sommerfeld solution to allow for nonparallel effects, but it is not clear how his approach can be adapted to incorporate nonlinear effects as well. Consistent theories that use the quasi-parallel nature of disturbances at large Reynolds numbers have been developed for the Blasius boundary layer by Smith (1979*a*) and Bodonyi and Smith (1981) that allow both nonlinearity and nonparallelism to be included. While these consistent theories are desirable from a theoretical viewpoint, they are less accurate in practical situations than Orr-Sommerfeld results which work well for Blasius flow even near the critical Reynolds number, *see* the direct numerical solutions of Fasel and Konzelmann (1990) and the careful experiments of Klingmann *et al.* (1993).

Nonetheless, it may ultimately be possible to construct composite approximations based on rational expansions that allow systematic treatment of nonparallel and nonlinear effects and that are as accurate as, or more accurate than, numerical Orr-Sommerfeld solutions. However, if this is to be achieved then careful consideration must be given to the choice of Reynolds number scalings that underpin the asymptotic theories. In Healey (1995*a*) numerical solutions to the Orr-Sommerfield equation were obtained over a wide range of Reynolds numbers so that the emergence of well defined scalings could be identified and compared with the asymptotic theories. The neutral curve was calculated and the behaviour of the eigenfunctions was also investigated. Through a consideration of the Reynolds number dependence of features in the eigenfunctions it was possible to identify the viscous wall layer and viscous critical layer of disturbances along the neutral curve. The main result was that a well defined Reynolds number exists where, on the upper branch of the neutral curve, the critical layer and wall layer merge. This point is marked by a kink in the neutral curve. This kink was first noticed by Reid (1965) in plane Poiseuille flow, but he conjectured that it might be an artifact of his asymptotic approximations. Hughes (1972) showed it to be a genuine feature of the Orr-Sommerfeld equation, but found no special behaviour associated with it, *see* also p. 190 of Drazin and Reid (1981). Hughes only looked at the real imaginary parts of the eigenfunctions, but Figure 5 of Healey (1995a) shows that the qualitative change can be seen by plotting the phase of the eigenfunctions.

The upper-branch asymptotic structure has a distinct critical layer separate from the wall layer, but this only occurs for Reynolds numbers higher than where the kink appears in the neutral curve. In the lower-branch asymptotic structure the critical layer overlaps the wall layer giving a "triple-decked" structure. This structure therefore obtains not only along the whole of the lower branch, but also along the upper branch until the kink is reached. The kink lies at such a high Reynolds number that transition over a flat plate is likely to be wholly determined by the lower branch structure and not the upper branch structure. This conclusion could not be reached from a consideration of the asymptotic theories alone and shows the usefulness of Orr-Sommerfeld solutions in clarifying the parameter regimes where the different asymptotic scalings apply. Nonlinear behaviour near the upper branch at Reynolds numbers above where the kink occurs is dominated by dynamics in the critical layer and can lead to integro-differential amplitude equations as first pointed out by Hickernell (1984). This behaviour is different from that near the lower branch which leads to the classical Landau equation, *see* Smith

(1979*b*). Note that the triple-deck structure near the lower-branch is largely unaffected by pressure gradients; it is the upper branch that is sensitive to any nonzero pressure gradient.

The boundary layer that develops over, say, an aeroplane wing experiences accelerating and decelerating external flows over different parts of the wing. In these regions the velocity profile is noninflexional and inflexional respectively. Rayleigh's inflexion point theorem tells us that in the former case the flow is stable to inviscid perturbations and is unstable for the latter. Viscosity can destabilize boundary layers and this provides a second instability mechanism for inflexional flows, and the main instability mechanism for noninflexional profiles. The nonslip condition at the wall introduces a viscous wall layer where subtle changes in phase between the horizontal and vertical perturbation velocities cause the Reynolds stress to become positive and energy to transfer from the mean flow into the perturbation. This viscous mechanism is independent of the inviscid mechanism whereby the singularity at the critical layer in the Rayleigh equation can also make a positive contribution to the Reynolds stress in inflexional profiles. The viscous instability can be associated with the lower branch of the neutral curve since here the instability is driven by the viscous wall layer and the critical layer contribution can be ignored at leading order. Inviscid instability is associated with the upper branch of the neutral curve since here the critical layer effects appear at leading order in the problem. The position of the upper branch in parameter space is fixed by the condition that the critical layer coincides with the inflexion point in the profile.

The distinction between inviscid and viscous instability thus seems straightforward; the flow is inviscidly unstable close to the horizontal part of the neutral curve (*i.e.* the part independent of Reynolds number) and is viscidly unstable close to the rest of the neutral curve where it has a Reynolds number dependence. But this simple categorization is unhelpful in practice. The strong growth of disturbances that initiates transition occurs in between the neutral curves; are these unstable waves viscous or inviscid in character? This question is irrelevant in the context of numerical Orr-Sommerfeld calculations since eigenvalues are obtained without needing to know about the instability mechanisms, but as indicated above, it does have consequences for nonlinear asymptotic theories.

In this paper, results will be presented of an investigation into the viscous-inviscid character of disturbances in Falkner-Skan boundary layers under conditions accessible to wind tunnel experiments. The unexpected conclusion is that even for relatively strong adverse pressure gradients, transition in wind-tunnel experiments seems likely to be driven by an essentially viscous instability mechanism despite the presence of the inflexion point.

It will be assumed that Orr-Sommerfeld theory is applicable to these boundary layers. Nonparallel effects become important at low Reynolds numbers, and the critical Reynolds number for instability in adverse pressure gradients is smaller than for the Blasius case. Also, decelerating boundary layers grow more rapidly in the streamwise direction and so, for both these reasons, these flows are expected to be more susceptible to non-parallel effects. However, the work of Govindarajan and Narasimha (1995) shows that although the neutral curves do become more sensitive to nonparallel effects for low Reynolds numbers and strong adverse pressure gradients, the effect on the integrated disturbance growth downstream is negligible. Therefore, the Orr-Sommerfeld theory provides a useful tool for determining the stability characteristics of boundary layers, even for adverse pressure gradients.

The results of calculations for the Blasius boundary layer are presented in § 2. While Healey (1995*a*) only presented results for the neutral curve, this section contains results for stable and unstable waves. It will be shown that plotting contours of constant relative growth, *i.e.* the growth rate per wavelength instead of a growth rate per displacement thickness or per metre, provides the clearest indication of scaling behaviour with Reynolds number. The kink found in the neutral curve is also shown to exist for contours of constant relative growth for nonneutral waves.

In § 3 it is shown that the kink persists for nonzero pressure gradients and still acts to mark the change in eigenfunction structure. For the adverse pressure gradients, the kink in the constant growth contours separates viscous from inviscid instabilities. This enables a graph to be plotted showing the Reynolds number at which the waves change from being entirely viscously unstable to where both viscous and inviscid unstable waves exists as a function of the strength of the pressure gradient parameter.

Although the inviscid behaviour moves to lower Reynolds numbers as the adverse pressure gradient gets stronger, the growth rates also increase and so transition will occur at lower Reynolds numbers too. To estimate whether the reduction in transitional Reynolds number precludes the measurement of an inviscid wave in a wind-tunnel experiment, net streamwise growth factors have been calculated for the particular experimental configuration of Seifert and Wygnanski (1995). Then, by finding the growth that has taken place up to the point at which transition was observed in the experiment it is possible to estimate by how much the freestream turbulence level would have to be reduced in order to maintain laminar flow at a Reynolds number large enough for inviscid waves to be measured. The results of these calculations are presented in § 4 and some conclusions are drawn in § 5.

2. Blasius boundary layer

The results in this section extend those in Healey (1995a), and establish a framework for the study of adverse pressure gradients. The Blasius boundary layer has a displacement thickness, δ, given by

$$\delta = 1.7208 \left(\frac{x \nu}{U_0} \right)^{1/2}, \tag{1}$$

where x is the streamwise coordinate (whose origin is at the leading edge), ν is the kinematic viscosity and U_0 is the freestream velocity. Physical quantities will be made dimensionless with δ, δ/U_0, U_0 and ρU_0^2 for the length, time, velocity and pressure scales respectively, where ρ is the density (assumed constant). The Reynolds number is defined as

$$R = \frac{\delta U_0}{\nu}. \tag{2}$$

The presence of x in (1) is due to the boundary layer growth and so the nondimensional frequency, ω, of a disturbance with fixed physical frequency, ω^*, increases as the disturbance propagates downstream. The nondimensional frequency F that is independent of x is given by

$$F = \frac{\omega^* \nu}{U_0^2} = \frac{\omega}{R}. \tag{3}$$

The experimental results of Seifert and Wygnanski (1995), which will be discussed in § 4, are based on the local displacement thickness and local freestream velocity and so the same variables have been used here to facilitate comparison.

Linearized wavy disturbances, $v(y)\, e^{i(\alpha x - \omega t)}$, are assumed to satisfy the Orr-Sommerfeld equation,

$$(\alpha U - \omega)(v'' - \alpha^2 v) - \alpha U'' v + \frac{i}{R}(v'''' - 2\alpha^2 v'' + \alpha^4 v) = 0 \tag{4}$$

where $U(y)$ is the mean flow (in this case the Blasius profile with its x dependence suppressed), y is the wall-normal coordinate (the wall lies at $y = 0$), primes denote differentiation with respect to y, v is the vertical component of the velocity perturbation and α is the wavenumber. In a spatial analysis ω is taken to be real and α is allowed to be complex and is determined by imposing the boundary conditions $v = v' = 0$ at $y = 0$

and as $y \to \infty$. The Orr-Sommerfeld equation has been solved using a compound matrix method due to Davey (1982) that can be used at very high Reynolds numbers. The core subroutines were kindly provided by Professor M. Gaster.

Figure 1 shows the Orr-Sommerfeld neutral curves plotted on log-log axes. The dotted and dashed lines are the leading order and four-term asymptotic expansions respectively for the neutral curves calculated in Smith (1979*a*) and Bodonyi and Smith (1981). These four-term expansions represent parallel flow approximations; nonparallel effects first appear in the 5th term of each expansion. The crosses are experimental results obtained by Klingmann *et al.* (1993). As well as showing excellent agreement with the Orr-Sommerfeld theory, they also indicate the parameter regime accessible to careful experiment. In fact the crosses lie in the range $490 < R < 1230$ and $100 < F \times 10^6 < 250$. Although higher R and lower F were attainable, the agreement with Orr-Sommerfeld results was already very good, which confirms that nonparallelism is negligible. Experiments on small amplitude disturbances in a laminar boundary layer at $R \approx 2000$ are possible in Gaster's low turbulence wind-tunnel, e.g. Healey (1995*b*), but the boundary layer in the same tunnel at $R \approx 2600$ shows intermittent turbulent spots (Shaikh, personal communicaiton); the former case corresponds to a metre from the leading edge when running at 18 ms^{-1} and the latter to a speed of 30 ms^{-1} at the same distance.

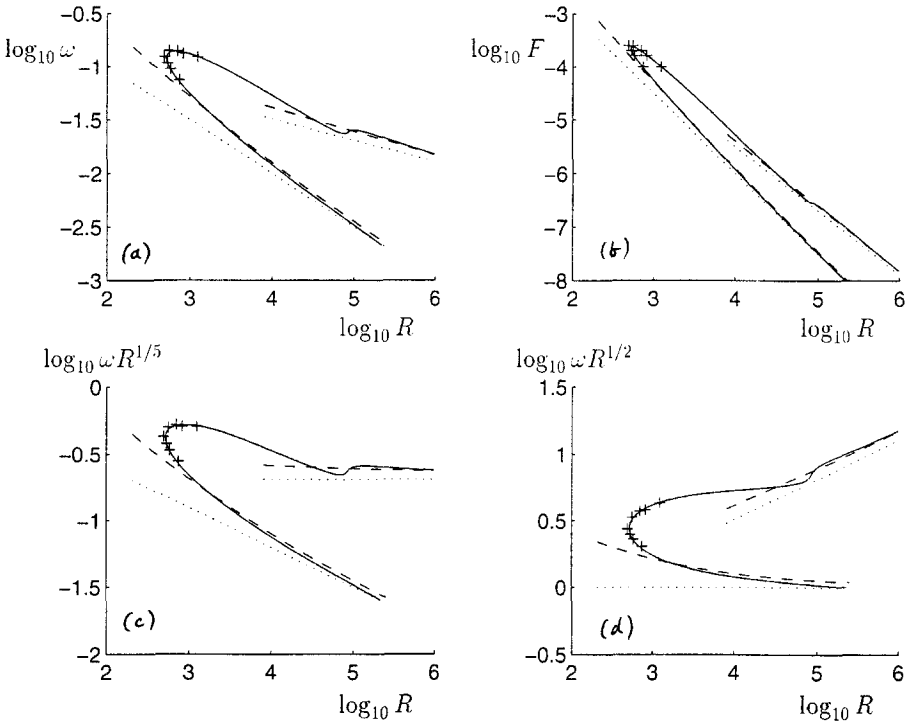

Fig. 1. – Solid lines are Orr-Sommerfeld neutral curves, "+" are experiments by Klingmann *et al.* (1993), dotted lines are leading order symptotic expansions and dashed lines are four term expansions from Smith (1979*a*) and Bodonyi and Smith (1981). (a) Is plotted using Orr-Sommerfeld variables, (b) using the nondimensional frequency that remains constant downstream, (c) is a scaling such that the upper branch becomes invariant as $R \to \infty$ and in (d) the lower branch becomes invariant as $R \to \infty$.

The kink in the upper branch near $R \approx 10^5$ is clear in Figures 1 a, c, d and the upper-branch expansions become inaccurrate for lower R. The kink is much less evident in Figure 1 b. The frequency F is often used in experimental work as disturbances then propagate along horizontal lines in the graph (instead of along parallel lines inclined at some angle as in the other plots). The change in scaling on either side of the kink is somewhat obscured in Figure 1 b, but this does not lessen its importance.

The change in asymptotic structure not only affects the neutral curve but also the contours of constant growth and decay rates shown in Figure 2. A band of strongly growing waves lies parallel to the lower branch. The width of this band is limited by kinks in the growth contours that together form a fault line across the graph. In the kink region for $R > 10^5$ the growth rates are relatively small and the eigenfunctions show both upper branch

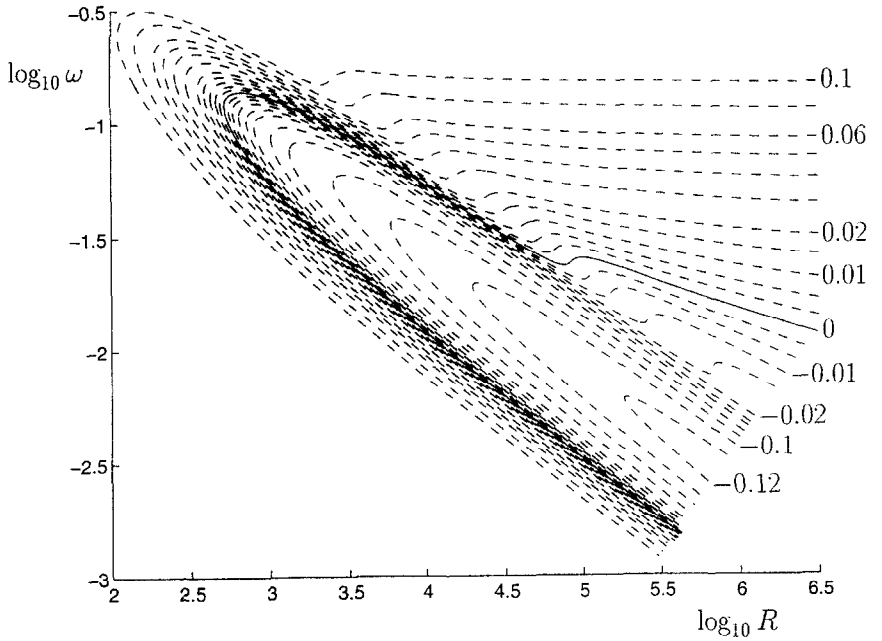

Fig. 2. – Growth rates for the Blasius boundary layer. The dashed lines are contours of constant α_i/α_r and the solid line is the neutral curve.

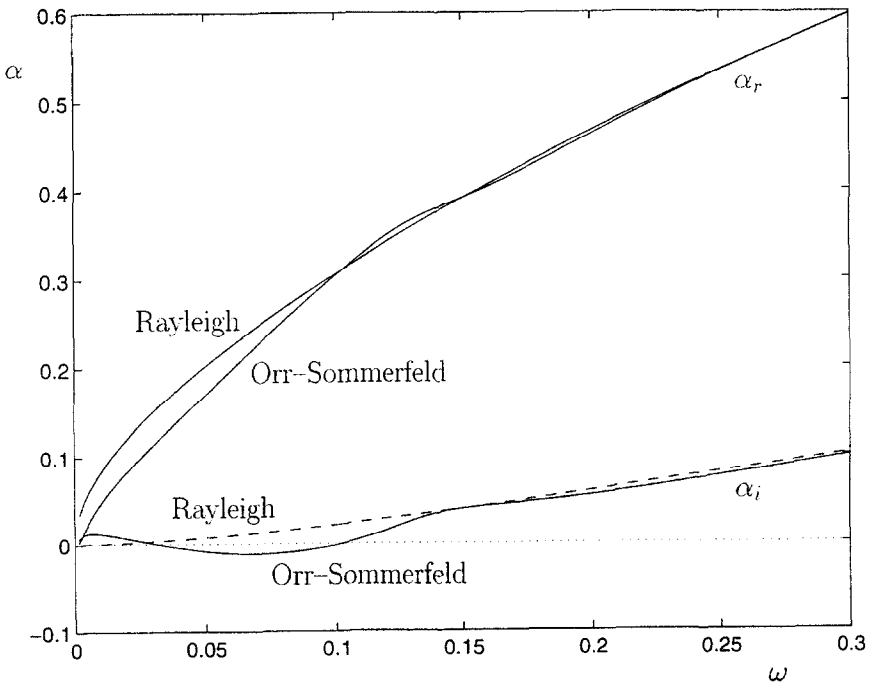

Fig. 3. – Comparison between inviscid Rayleigh calculations and viscous Orr-Sommerfeld calculations at R=2000 (the dotted line shows α_i=0).

and lower branch characteristics, and so can be associated with the high-frequency limit of the triple-deck theory discussed in Smith and Burggraf (1985). For high enough frequencies the contours are approximately horizontal and so correspond to damped inviscid waves. This has been verified by solving the Rayleigh equation and comparing the eigenvalues with those obtained from the Orr-Sommerfeld equation, *see* Figure 3. The details of the Rayleigh computations are given in Appendix A. At this R both the real and imaginary parts of the wavenumbers are in close agreement for $\omega > 0.15$ confirming the inviscid nature of these waves. For lower ω the imaginary part is significantly modified by viscosity giving the band of viscous instability waves.

Note that the shape of the contours changes dramatically if different defintions for the growth rate are used. If α_i is used (growth per displacement thickness) then the maximum growth occurs at $R \approx 4930$, $\omega \approx 0.0463$ with a small local maximum in growth at $R \approx 694000$, $\omega \approx 0.00880$ (in the kink region). If $\alpha_i' = \alpha_i^* \nu/U_0 = \alpha_i/R$ is used (growth per metre) then the strongest growth occurs at $R \approx 1050$, $\omega \approx 0.0920$. The contours of α_i and α_i' thus form closed loops for the unstable waves, which makes the Reynolds number scalings more difficult to identify. However, the overall picture is always the same with the strongest growth rates near the lower branch.

Figure 2 shows that for $R > 10^5$ there is a wedge of weakly growing waves near the upper branch. In fact, this wedge covers a greater part of the plate than the more unstable waves near the lower branch, and Figure 4 shows this by plotting the growth rates for constant values of F using a linear scale for the nondimensional distance from the leading edge. The area under these curves gives the negative of the logarithmic growth of the disturbances. Figure 4a confirms the asymptotic description given in Goldstein and Durbin (1986), *i.e.* there is a relatively narrow band of strongly growing waves close to the lower branch, followed by the main unstable

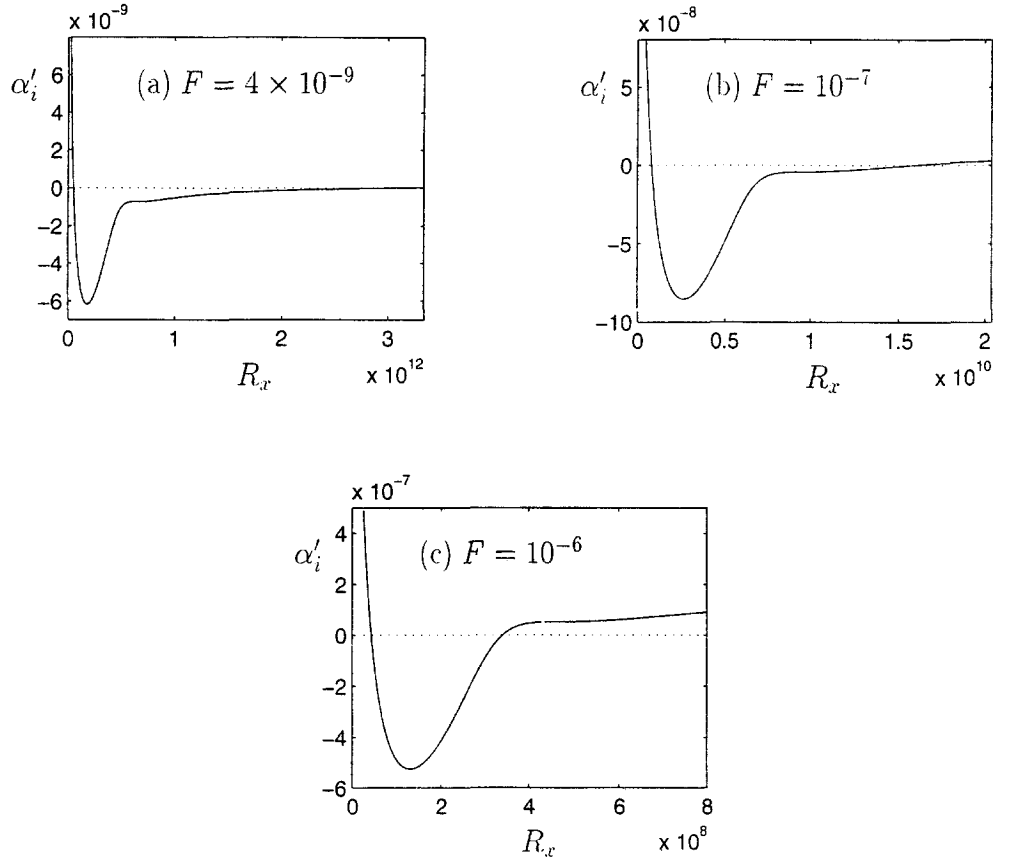

Fig. 4. – The variation of growth rate with downstream distance for three values of F, where $\alpha_i' = \alpha_i^* \nu/U_0 = \alpha_i/R$ is the "growth rate per metre" and $R_x = x U_0/\nu = (R/1.7208)^2$ is the nondimensional distance from the leading edge (the dotted line shows $\alpha_i = 0$).

region that covers most of the plate and where the growth rates are small. However, as F is increased, this situation changes. Figure 4b shows the weak growth region near the upper branch covering a similar extent to that of the strong growth region near the lower branch. In Figure 4c the entire unstable region is covered by the strongly growing lower branch part. The low R_x part of Figure 4c may be relevant to a wing in flight conditions, but the R_x in Figures 4a,b correspond to distances hundreds and thousands of times further downstream, and so have no relevance to aeronautical applications.

However, the link in the neutral curve is sensitive to the pressure gradient imposed on the boundary layer, and moves to lower R in an adverse pressure gradient. In the following sections corresponding results are presented for adverse pressure gradient flows. The kink then marks the point where inviscid behaviour takes over from viscous behaviour.

3. Adverse pressure gradients

The principal effect of imposing a pressure gradient on a boundary layer is to modify the mean velocity profile. Favorable pressure gradients increase $U'(0)$ and lead to negative $U''(0)$ and adverse pressure gradients decrease $U'(0)$ and lead to positive $U''(0)$. Far from the wall $U'' < 0$ and so an inflexion point exists in the latter case. The effect of these changes on the stability can be briefly summarized as follows.

Near the lower branch the disturbances have a triple-deck structure and the Reynolds stresses in the lower deck (the viscous wall layer), where the nonslip condition at the wall is satisfied, can cause instability. In this deck the velocity profile can be replaced by a straight line to leading order with gradient $U'(0)$. Thus neither adverse nor favorable pressure gradients have an important effect as long as the flow is not close to separation. The scalings are unaffected ($\omega_n \propto R^{-1/2}$ where ω_n is the neutral frequency) and there is only a change to the numerical values of the coefficients of proportionality.

However, near the upper branch the critical layer (where the phase speed matches the local mean flow speed) plays a determining role in the stability. In the inviscid theory there is a phase jump across the critical layer that makes a contribution to the Reynolds stress that is proportional to the profile curvature at the critical layer, U_c''. For favourable pressure gradients U_c'' is finite and negative and the neutral curve occurs when this stabilizing influence is balanced by the destabilizing effect of the viscous wall layer. This happens at $\omega_n \propto R^{-1/3}$, with a constant of proportionality dependent on the strength of the pressure gradient. For Blasius flow U_c'' is small and negative and the neutral curve lies at $\omega_n \propto R^{-1/5}$. In an adverse pressure gradient U_c'' is zero at the neutral curve with $\omega_n = \text{const}$. Thus even very small favorable and adverse pressure gradients have a major effect on the upper branch neutral curve and the Blasius flow is a special case of viscous instability with its own scalings.

This behaviour is illustrated in Figures 5 and 6. The overall pictures are barely changed from that in Figure 2, but closer inspection reveals that the upper branch, beyond the kink, is very sensitive to the pressure gradient and follows the different scalings described above. The band of strongly growing lower branch waves are not significantly affected by the pressure gradient, but do become slightly more unstable for adverse pressure gradients.

These results imply that these small pressure gradients would not be significant for values of R encoutered in experiments where the instability is likely to always be viscous. However, even small pressure gradients *are* known to have a strong effect on experiments. Ross *et al.* (1970) produced a set of experimental estimates for the neutral curve in Blasius flow and these results provided a curve in Blasius flow and these results provided a bench mark for subsequent theoretical calculations for over 20 years. They found a discrepancy with the Orr-Sommerfeld theory at low R and attributed it to nonparallel effects. Various attempts have been made to construct nonparallel theories to account for this discrepancy. However, Saric (1990) suggested that the lowest R results might have been affected by the adverse pressure gradient recovery zone near the leading

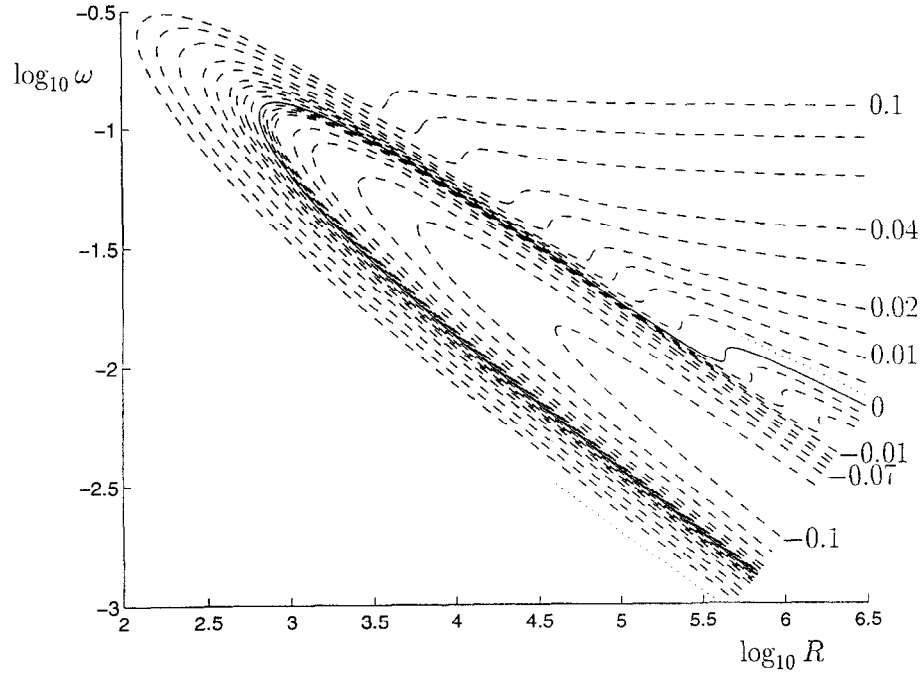

Fig. 5. – Growth rates for a small favourable pressure gradient $m = 0.01$. The dashed lines are contours of constant α_i/α_r and the solid line is the neutral curve. The pressure gradient parameter m corresponds to a freestream velocity $U_0 \propto x^m$.

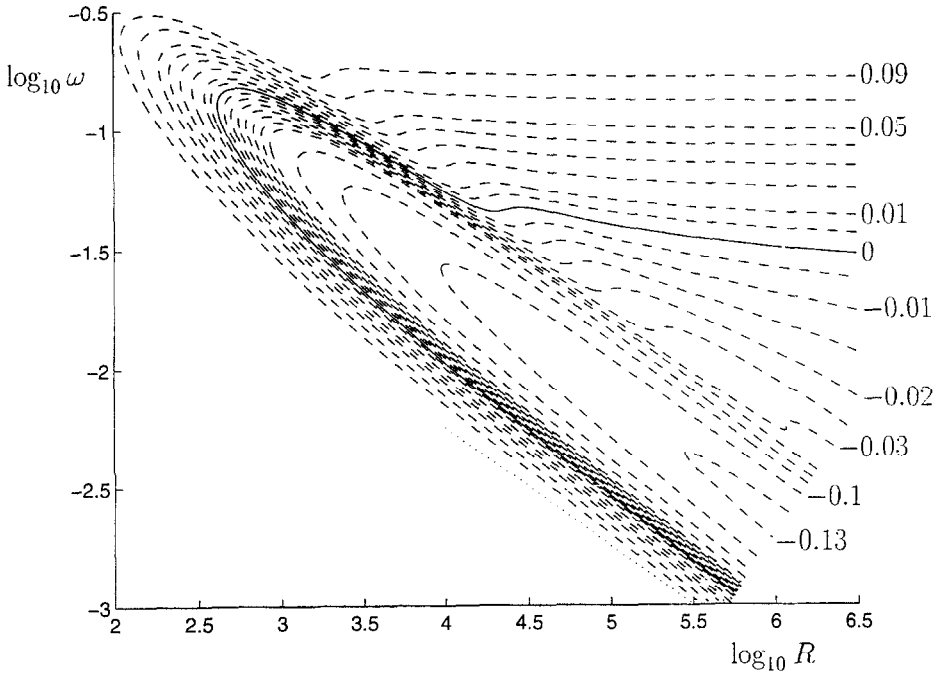

Fig. 6. – Same as Figure 5, but for a small adverse pressure gradient $m = -0.01$.

edge. Klingmann *et al.* (1993), with careful leading edge designs and pressure gradient measurements, obtained experimental results lying much closer to the Orr-Sommerfeld neutral curve, *see* Figure 1. They also introduced a small adverse pressure gradient that would have been indistinguishable from zero in the Ross *et al.* experiments.

The neutral curve then moved to a position similar to that found by Ross *et al.* Figure 11 of Healey (1995*a*) shows that the same adverse pressure gradient as used in Figure 6 causes the neutral curve to pass through Ross' data near the critical Reynolds number for instability. Therefore, pressure gradients of this magnitude are measurable and cause significant effects in experiments.

Small pressure gradients are important in both experiment and theory, but for different reasons. In experimental situations the chief effect is the modification of the coefficients multiplying the lower-branch scalings; this does not alter the basic viscous instability mechanism. In the theory, however, pressure gradients are crucial because they change the upper-branch asymptotic scalings and hence the physics of the instability, e.g. inviscid instabilities. In this sense, experimentalists and theorists may be talking at cross-purposes when they each refer to the importance of pressure gradients to stability.

Figures 2, 5 and 6 also show that the position of the kink, which marks the change from viscous to inviscid instability, moves to lower R for an adverse pressure gradient. Figure 7 shows the stability curves for $\beta = -0.12$, where $m = \beta/(2-\beta)$. Note that quantities have still been made dimensionless using displacement thickness, but this is no longer given by (1). This value of β is relevant to the experimental work discussed in § 4; separation occurs at $\beta \approx -0.1988$.

The diagonal band of strongly growing waves corresponds to the viscous instability and horizontal contours are where the instability is inviscid. There is still a relatively well defined boundary between these two regions. Note that, contrary to what is often assumed, the most unstable waves are viscous and not inviscid. Dovgal, Kozlov and Michalke (1994) investigated the stability of various profiles corresponding to laminar flows close to separation. They calculated stability characteristics at several Reynolds numbers and also for inviscid flow. Their Figures 12 and 14 show that the phase velocity is essentially independent of Reynolds number and hence is inviscid even at low Reynolds numbers. This agrees with our results shown in Figure 3 where the real parts

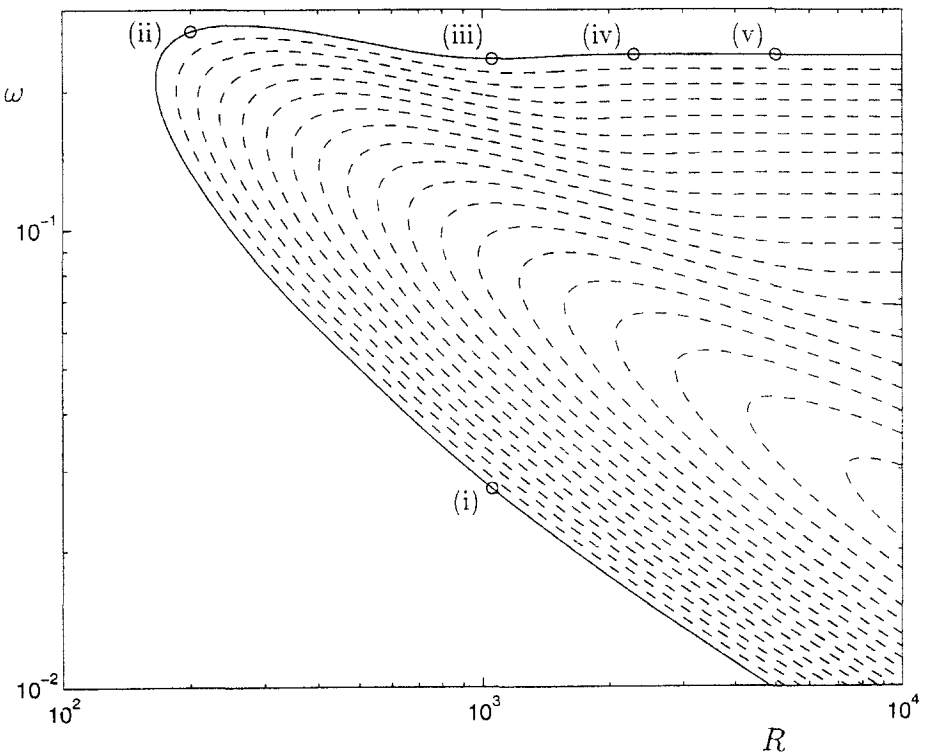

Fig. 7. – Neutral curve (solid line) and contours of constant growth α_i/α_r (dashed lines) for $\beta = -0.12$.

of the Orr-Sommerfeld eigenvalues are qualitatively similar to the Rayleigh eigenvalues even for Blasius flow. However, Figure 13 of Dovgal *et al.* shows that the imaginary parts are sensitive to Reynolds number at low frequencies, which corresponds to the viscous nature of these waves, and they become independent of Reynolds number at higher frequencies, showing the inviscid nature of these waves. Therefore, the results in Figure 7 are in agreement with those in Dovgal *et al.*

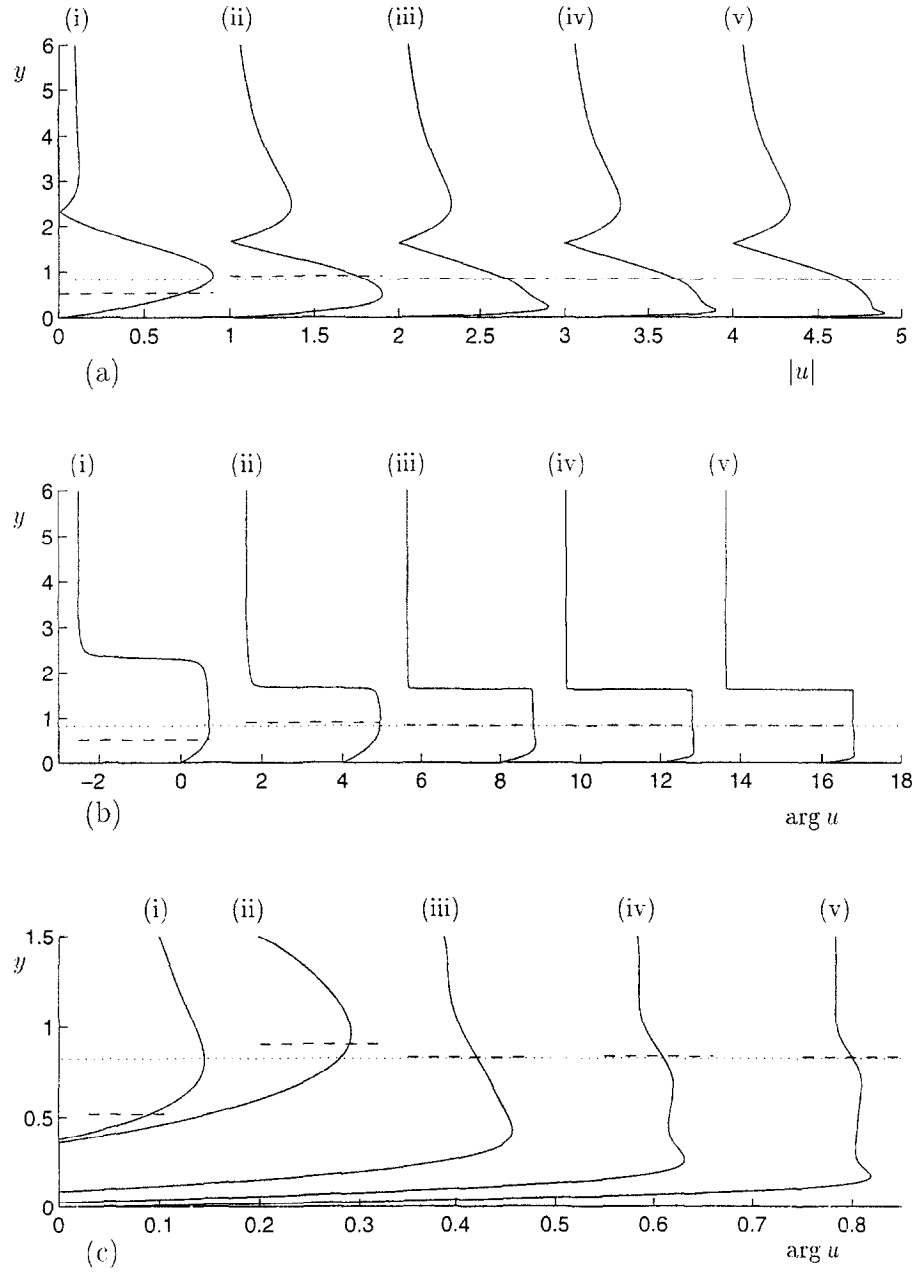

Fig. 8. – Eigenfunctions at the points on the neutral curve marked on Figure 7 where u is the horizontal velocity perturbation. (a) Shows their normalized magnitudes, (b) and (c) show the phases in radians on different scales. The dotted line indicates the height of the inflexion point in the mean velocity profile and the dashed lines show the height where $U = \omega/\alpha$. The values of R and ω for (i) to (v) are $R = 1051$, 200, 1051, 2296, 5000 and $\omega = 0.0273962$, 0.269297, 0.234587, 0.23958, 0.23902 respectively.

The circles labelled (iii) and (iv) lie on a local minimum and maximum respectively of the graph of the neutral curve and so correspond to the remnants of the kink. Figure 8 shows the magnitudes and phases of the eigenfunctions at the points labelled by the circles in Figure 7. The magnitude of the eigenfunctions is shown in Figure 8a and the phases in Figures 8b, c. The magnitudes for (i) and (ii) show a weak outer maximum and a stronger inner maximum and so are qualitatively similar to Blasius eigenfunctions, as expected for viscous waves. Note that the eigenfunctions can have more complicated shapes near separation and away from the neutral curve, as shown by Dovgal, Kozlov and Michalke (1994). The magnitude drops to zero between the maxima

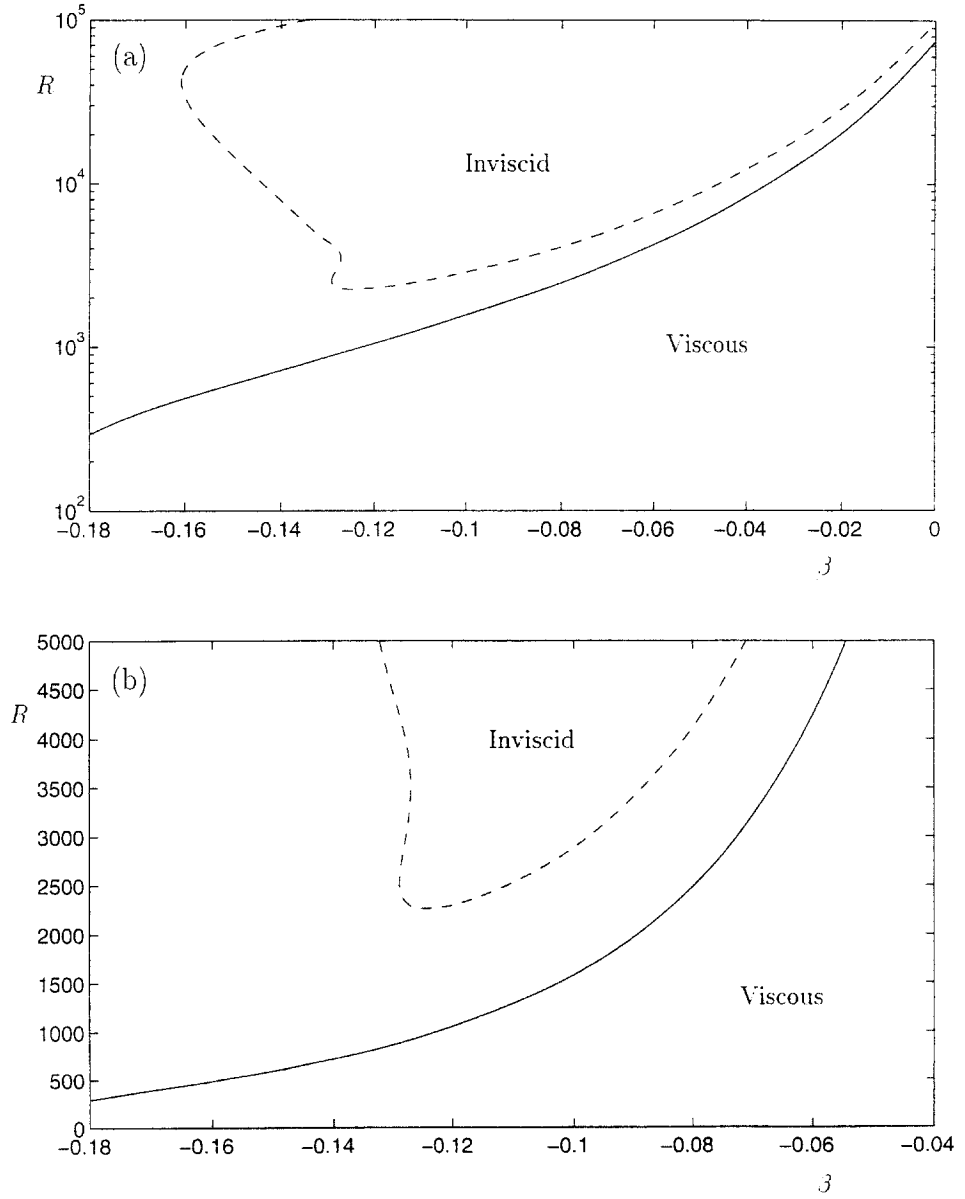

Fig. 9. – For small β the kink on the upper branch of the neutral curve is characterized by a local maximum and minimum which lie close together in the neutral curve. The dashed lines and solid lines show the position of these maxima and minima respectively as a function of β. Near $\beta = -0.13$, where the dashed line turns back on itself, it still represents extrema, but of both types.

as the eigenfunction changes sign, and this corresponds to the π phase jump in Figure 8b. The eigenfunction at (v) was taken from the inviscid part of parameter space. Its magnitude shows a sharp maximum very close to the wall and this corresponds to the viscous wall layer. The phase in Figure 8c shows a rapid variation in the viscous wall layer and also a small jump across the critical layer. The critical layer now lies very close to the inflexion point in the profile which is consistent with inviscid theory. The critical layer phase jump is only of order 0.025 radians (1.4 degrees) and so would be difficult to detect in an experiment.

The emergence of the critical layer as a distinct structure takes place between (iii) and (iv), *i.e.* within the kink region of the neutral curve. This was also the case for the Blasius profile and suggests that the position of the kink can be relied upon to indicate the onset of inviscid behaviour over a range of pressure gradients. Figure 9 shows how the local minimum and maximum associated with the kink vary with R. For example, unstable linear inviscid behaviour can occur for $R < 3000$ provided $\beta < -0.1$, but it will only be observed in an experiment if the viscous instabilities have not already caused sufficient growth of background disturbances to bring about a transition to turbulence at a lower values of R. To discover whether this is likely or not, growth rates have been calculated in § 4 using boundary layer data from the experiment on transition in an adverse pressure gradient presented in Seifert and Wygnanski (1995).

TABLE I. – Height of the inflexion point d measured in units of momentum thickness, θ, and displacement thickness, δ. H is the shape factor.

β	H	d/θ	d/δ
0.0	2.591100	0.0	0.0
– 0.05	2.675759	1.472097	0.550160
– 0.10	2.801115	2.132799	0.761411
– 0.12	2.871776	2.367600	0.824437
– 0.15	3.020940	2.727381	0.902825
– 0.17	3.178448	3.005196	0.945491
– 0.18	3.296727	3.178048	0.964001
– 0.19	3.480794	3.412914	0.980499
– 0.198	3.833671	3.803365	0.992095
– 0.198838	4.029226	4.002633	0.993400

The results in Figure 9 can be adapted for use with the more general, nonsimilar, profiles that arise in situations of practical interest. The critical layer for a neutral wave on the upper branch lies at the inflexion point, and the width of this layer, and that of the wall layer, each depend on inverse powers of the Reynolds number. In an arbitrary profile, the height of the inflexion point therefore plays a key role in determining the Reynolds number at which these layers merge. Table 1 shows how the height of the inflexion point varies with β. The height measured with respect to momentum thickness gives the most sensitive dependence on β. It may be that a good estimate of the Reynolds number at which the layers merge can be obtained by taking the height of the critical layer and using the table to interpolate to the corresponding value of β to be used in Figure 9.

4. Growth rates in a decelerating boundary layer

There have been a number of experimental investigations into adverse pressure gradient boundary layers, for example the study by Wubben, Passchier and Van Ingen (1990) where a flow with $\beta = -0.14$ was maintained over a flat plate in the working section of the wind tunnel. Transition occured about 700 mm from the leading edge as detected by the change in shape factor. Although profiles are plotted and compared with similarity profiles, neither displacement nor momentum thicknesses were quoted, and so the Reynolds number at transition could not be estimated accurately, but is probably in the range 1300 to 2000. The freestream turbulence was

0.05%. More detailed information is available from the experiment by Seifert and Wygnanski (1995). We shall focus on this experiment, but the method used here could be applied to any experiment.

They studied the evolution of a wavepacket generated by a point source in a boundary layer subjected to an adverse pressure gradient. Hot-wire measurements were taken over a flat plate, and a flexible faring was placed near the wall opposite the plate. The faring could be adjusted at a number of streamwise positions with screw-jacks so that the desired self-similar adverse pressure gradient could be maintained over the working part of the plate. This arrangement eliminates surface curvature effects from the boundary layer.

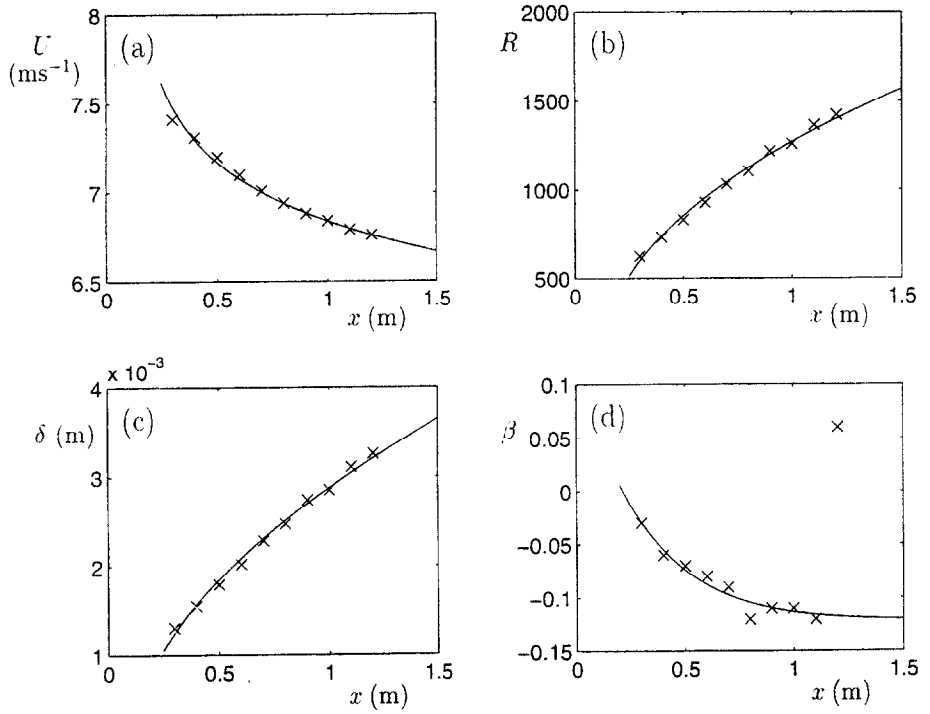

Fig. 10. – Crosses are experimental data for the boundary layer studied by Seifert and Wygnanski (1995), solid lines are given by (5)-(8).

Figure 10 shows the boundary layer data from this experiment. The freestream velocity was measured using a pitot tube, the displacement thickness by integrating measured hot-wire velocity profiles and β was estimated by fitting Falkner-Skan profiles to the measured profiles. The Reynolds number is based on local freestream velocity and local displacement thickness. The variation of β with x shows that the profiles are not self-similar over the whole plate. However, in order to extrapolate further downstream, it will be assumed here that the pressure gradient parameter would have approached a constant value β_0 with increasing downstream distance if a laminar flow could have been maintained. In fact, the boundary layer became transitional at $x \approx 1.2\,\mathrm{m}$ and the profiles start to deviate significantly from the laminar similarity flow for larger x. The curves in Figures 10a, c, d were obtained by fitting coefficients to the crosses and are given by

$$U = 6.79\,(x - x_0)^{\beta_0/(2-\beta_0)} \tag{5}$$

$$\delta = 3.08 \times 10^{-3}\,(x - x_0)^{(1-\beta_0)/(2-\beta_0)} \tag{6}$$

$$\beta = \beta_0 + (0.239 - 0.157\,x)\,e^{-x/0.4}, \tag{7}$$

where $\beta_0 = -0.12$, $x_0 = 0.12$ m, x is given in metres and R is obtained as a function of x by substituting (5) and (6) into (2) with $\nu = 1.55 \times 10^{-5}$ m^2 s^{-1} to give

$$R = 1350\,(x - x_0)^{1/(2-\beta_0)}. \tag{8}$$

The most downstream value for β was not used in the fit.

At a given x the eigenvalues are calculated using (7) and (8) and the dimensional frequency and growth rate are calculated using (5) and (6). Figure 11 shows the neutral curve and contours of constant dimensional growth rates calculated using (5)-(8); the apparent indpendence of the lower branch with Reynolds number

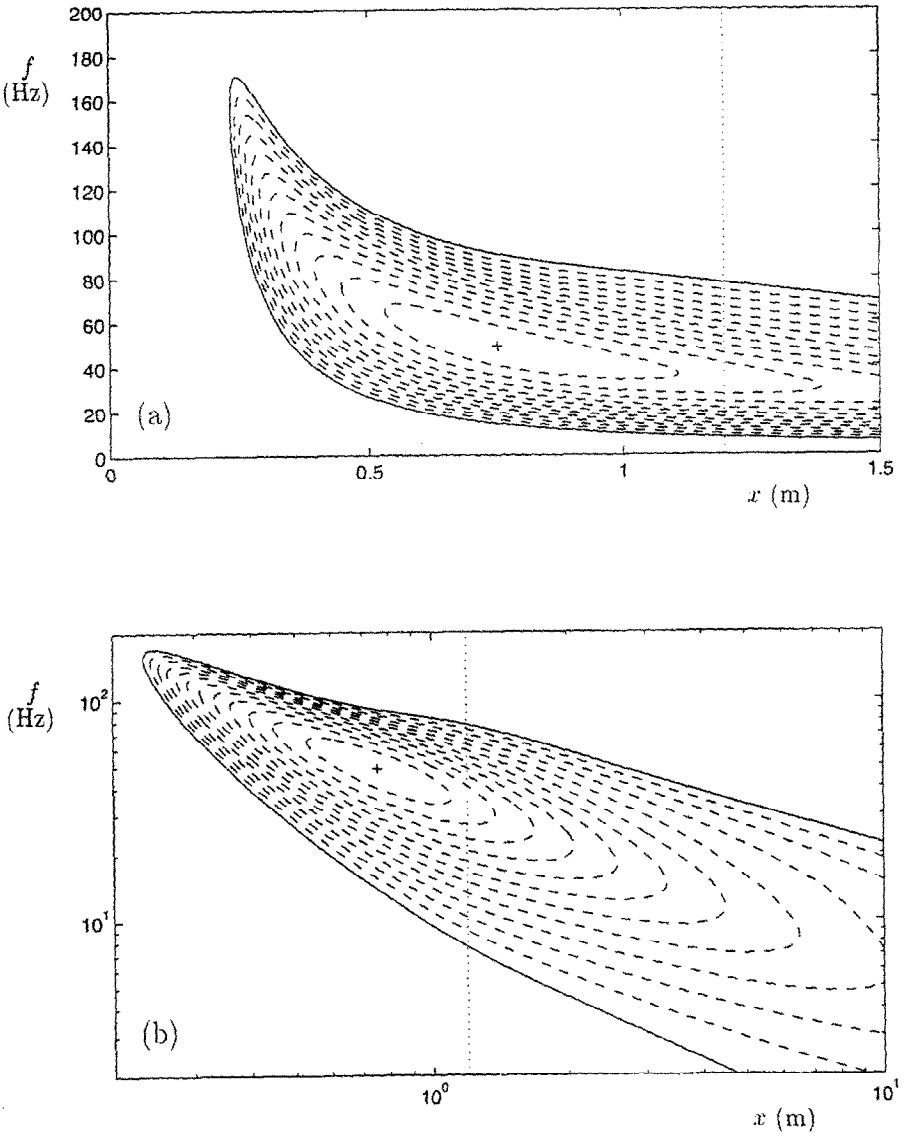

Fig. 11. – Neutral curve (solid line) and contours of constant dimensional growth α_i^* (dashed lines) which decrease in steps of -1 m^{-1} to -11 m^{-1}. f and x are the dimensional frequency and downstream distance respectively calculated using (5)-(8) for the boundary layer of Seifert and Wygnanski (1995). The fastest growing waves lies at the "+" where $f = 48.9$ Hz, $x = 0.755$ m and $\alpha_i^* = -11.8$ m^{-1}. The vertical dotted line corresponds to where the boundary layer became transitional in the wind-tunnel experiment.

in Figure 11 a is an artifact of using linear scales, Figure 11 b shows its scaling more clearly. More accurate stability calculations could be achieved by numerically solving the boundary layer equations with the freestream velocity from the experiment. This may be useful for making detailed comparisons with the experiment, but here we assume that the Falkner-Skan profiles will give a good enough approximation to the flow to give the correct qualitative picture. Frequencies above 100 Hz are all damped beyond 0.5 m downstream and the fastest growing wave has frequency close to 50 Hz and occurs near $x = 0.75$ m. However, the lower the frequency the greater the eventual net growth, as illustrated in Figure 12. The position at which transition occured in the experiment corresponds to a growth factor of e^8 (note that three-dimensional waves are also present in the experiment, so this may be an underestimate). At this point $R \approx 1400$, $\beta \approx -0.12$ and so from Figures 7 and 9 disturbances near the upper branch are beginning to show inviscid characteristics. Figure 11 a shows that at transition the upper branch corresponds to 75 Hz, but Figure 12 shows that at the same value of x there are disturbances at 45 Hz that have amplitudes of order 50 times larger. Thus the viscously unstable waves are significantly larger than the inviscid waves, and these viscous waves are still growing strongly, while the inviscid waves will start to decay according to linear theory.

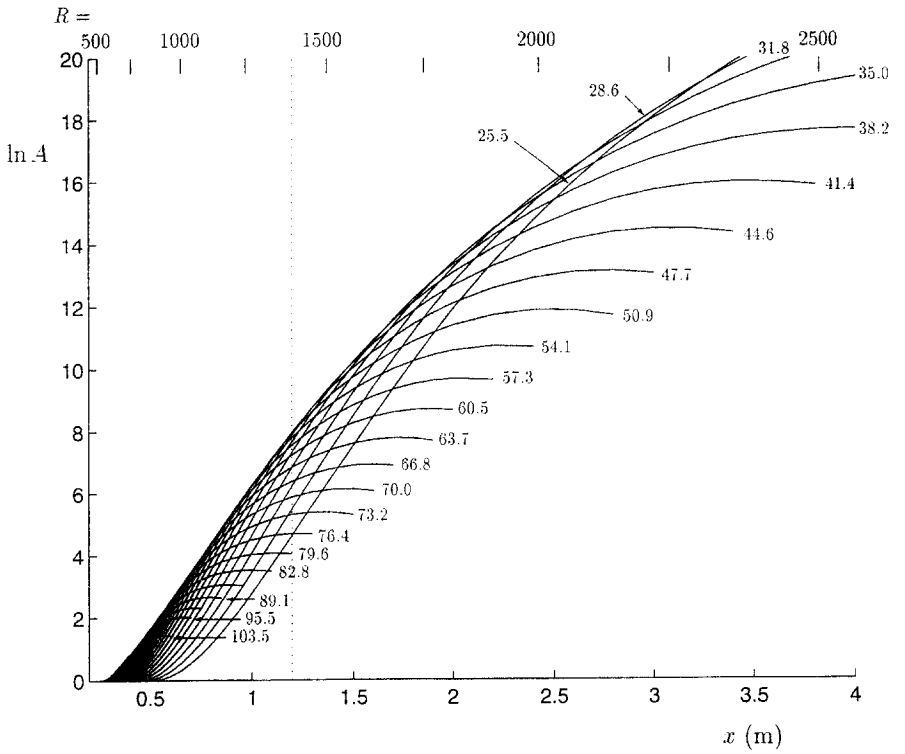

Fig. 12. – Growth curves for disturbances with constant physical frequency (measured in Hz) in the boundary layer of Seifert and Wygnanski (1995). The vertical dotted line shows where the boundary layer became transitional in the experiment. A is the amplitude of the disturbance normalized to unity as the disturbance crosses the lower branch of the neutral curve. The vertical bars along the top of the figure show values of R increasing in steps of 250.

The inviscid waves could be studied by carrying out an experiment where, say, a 75 Hz exciter was used to generate waves 50 times larger than the background disturbances at input so as to give signals comparable to the background noise by the time they have reached the upper branch (ensemble averaging can then be used to improve the signal to noise ratio). However, this would be difficult to achieve in practice. Seifert and

Wygnanski quote a freestream turbulence level of 0.03%, so the input must be at least 1% of the freestream and Seifert (1996) has already shown that amplitudes much smaller than this lead to nonlinearity for 60 Hz harmonic forcing. Furthermore, Figure 8 a, b shows that the eigenfunctions between (iii) and (iv) are almost indistinguishable from one another, hence it would be hard to detect the subtle differences in the eigenfunctions between viscous and inviscid instability.

Even if a sufficiently clean freestream environment can be attained that delays transition to higher R (perhaps during flight conditions), Figure 12 shows that near the upper branch (maxima in the constant frequency curves) there is always a lower frequency wave with larger amplitude. For example, a 45 Hz wave reaches the upper branch at $x \approx 3$ m and at this point the 29 Hz wave is about 50 times bigger. However, sufficiently far downstream the net growth across the triple-deck region is less than that across the inviscid region, *see* Cowley and Wu (1993), so inviscid waves will dominate sufficiently far dowstream. Nonetheless, for inviscid waves whose growth factor is less than e^{20}, *i.e.* for any case of practical interest, there will be lower frequency, faster growing, viscous waves with amplitudes some 50 times larger.

5. Conclusions

The stability of adverse pressure gradient boundary layers has been investigated using Orr-Sommerfeld theory. A kink lies on the upper branch of the neutral curve and a study of the phase of the eigenfunctions in the wall normal direction reveals that, for R higher than where the kink appears, there is a well defined jump in phase at the height of the critical layer. For lower R the critical layer lies within the viscous wall layer and the phase jump is not seen. The kink thus acts as boundary between viscous and inviscid regions. The position of the kink on the upper branch depends upon the strength of the pressure gradient, and this has been exploited in Figure 9 to give a graph showing the Reynolds number above which inviscid instability exists as a function of β. For β small or zero, the disturbances are viscous and triple-decked at realistic R. The experiments of Seifert and Wygnanski (1995) show that waves with inviscid characteristics just emerge before transition for $\beta \approx -0.12$. If this trend continues then experiments on inviscid waves may be feasible in stronger adverse pressure gradients, e.g. in the experiment of Wubben *et al.* (1990); however boundary layer separation occurs at $\beta = -0.1988$.

It seems that inviscid waves might be observed experimentally (using ensemble averaging techniques), but in natural transition there are lower frequency viscous waves that have amplitudes 50 times larger than the inviscid waves (at least for waves with growth factors less than $e^{20} \approx 5 \times 10^8$). On the other hand, perhaps the simultaneous emergence of inviscid waves and transition in the experiment is not coincidental? If it could be demonstrated that the nonlinear growth of inviscid waves is sufficiently stronger than the nonlinear growth of viscous waves, even when the inviscid waves have 1/50th the amplitude, then this would be a significant discovery. This hypothesis could be tested with further experiments, numerical simulations and theory. However, Figure 8 shows that the linear disturbance structure changes only slightly from viscous to inviscid regions, so on this evidence, it is difficult to see how the inviscid waves could evolve so differently from the viscous waves at finite R, despite the differences implied by asymptotic theories.

Acknowledgements. – I am grateful to Dr Avi Seifert for providing me with raw data from his experiments on boundary layers in an adverse pressure gradient. I thank one of the referees for providing the data presented in Table 1, and for their comments on the importance of the height of the inflexion point. This work was supported by a grant from the Engineering and Physical Sciences Research Council of the UK under its Applied Nonlinear Mathematics Initiative.

APPENDIX A

A few details concerning the spatial solutions to the Rayleigh equation are presented in this Appendix. The damped solutions that correspond to viscous solutions are obtained by choosing an integration contour that passes below the critical point y_c defined by $\alpha U(y_c) = \omega$, *see* (11) below. Thus $U(y_c)$ is complex and so y_c must be continued into the complex plane. This has been achieved by solving the Blasius similarity equation,

$$2f''' + ff'' = 0, \tag{9}$$

with boundary conditions $f(0) = f'(0) = f'(\infty) - 1 = 0$ where $f'(\eta) = U(y)$ but with all the variables taken to be complex. The similarity variable is defined by $\eta = 1.7208\, y^*/\delta$ using (1). Equation (9) was integrated along the path

$$\eta_i = \frac{-d\eta_r\,(6 - \eta_r)\, e^{-\eta_r}}{1.871213} \tag{10}$$

from $\eta_r = 0$ to $\eta_r = 6$, where $\eta = \eta_r + i\,\eta_i$ and the numerical factor was chosen so that the maximum deviation into the complex plane is $-d$ (which occurs at $\eta_r = 0.837722$). The value $\eta_r = 6$ was to chosen to give a finite outer boundary condition for which U has almost reached its asymptotic value.

This procedure provides complex values of U and U'' directly for any given value of d. The precise form of (10) is unimportant as long as the path lies below y_c. The Rayleigh equation,

$$\left(\frac{\alpha U''}{\alpha U - \omega} + \alpha^2\right) v - v'' = 0, \tag{11}$$

is then solved by shooting for complex α for a given real ω, with the boundary conditions $v = 0$ at $y = 0$ and $v = e^{-\alpha y}$ at the outer boundary. It is not known *a priori* what value d should take, but it was found that if it was too small then (11) converged to a spurious solution where y_c lies on the path of integration, and thus would not be resolved properly. This eventuality was tested for and d increased until the path passed under y_c and the eigenvalues become independent of the path. However, a simple relation for giving suitable d was discovered. If the real part of U is plotted against η_r (giving a projection of the complex profile) then this profile was found to become inflexional when $d = d_0 \approx 0.313$. When $\omega = 1$ it was found that the condition $d > 0.616$ had to be satisfied to get nonspurious eigenvalues, and that in fact the condition $d > 2\,\omega\, d_0$ applies over a wide range of ω. The significance of this observation is not understood.

This method of obtaining solutions to Rayleigh's equation was suggested to me by Prof. M. Gaster (personal communication, 1993) and, subsequent to the present work, it was extended by Lingwood (1995) for use with three-dimensional profiles in her work on the absolute instability of the boundary layer over a rotating disc.

REFERENCES

BODONYI R. J., SMITH F. T., 1981, The upper branch stability of the Blasius boundary-layer, including non-parallel flow effects, *Proc. R. Soc. Lond.*, **A 375**, 65-92.

COWLEY S. J., WU X., 1993, Special course on progress in transition modelling, *AGARD Rep. 793*.

DAVEY A., 1982, A difficult numerical calculation concerning the stability of the Blasius boundary layer. In *Proc. 2nd Symp. o Stability in the Mechanics of Continua*, Schroeder F. H. ed., Springer-Verlag, 365-372.

DOVGAL A. V., KOZLOV V. V., MICHALKE A., 1994, Laminar boundary layer separation: Instability and asociated phenomena, *Prog. Aerospace Sci.*, **30**, 61-94.

DRAZIN P. G., REID W. H., 1981, *Hydrodynamic Stability*, Cambridge University Press.

FASEL H., KONZELMANN U., 1990, Nonparallel stability of a flat-plate boundary-layer using the complete Navier-Stokes equations, *J. Fluid Mech.*, **221**, 311-347.

GASTER M., 1974, On the effects of boundary-layer growth on flow stability, *J. Fluid Mech.*, **66**, 465-480.

GOLDSTEIN M. E., DURBIN P. A., 1986, Nonlinear critical layers eliminate the upper branch of spatially growing Tollmien-Schlichting waves, *Phys. Fluids*, **29**, 2344-2345.

GOVINDARAJAN R., NARASIMHA R., 1995, Stability of spatially developing boundary-layers in pressure-gradients, *J. Fluid Mech.*, **300**, 117-147.

HEALEY J. J., 1995*a*, On the neutral curve of the flat-plate boundary-layer: comparison between experiment, Orr-Sommerfeld theory and asymptotic theory, *J. Fluid Mech.*, **288**, 59-73.

HEALEY J. J., 1995*b*, A new boundary-layer resonance-enhanced by wave modulation: theory and experiment, *J. Fluid Mech.*, **304**, 231-262.

HICKERNELL F. J., 1984, Time dependent critical layers in shear flows on the beta-plane, *J. Fluid Mech.*, **142**, 431-449.

HUGHES T. H., Variable mesh numerical method for solving the Orr-Sommerfeld equation, *Phys. Fluids*, **15**, 725-728.

KLINGMANN B. G. B., BOIKO A. V., WESTIN K. J. A., KOZLOV V. V., ALFREDSSON P. H., 1993, Experiments on the stability of Tollmien-Schlichting waves, *Eur. J. Mech., B/Fluids*, **12**(4), 493-514.

LINGWOOD R. J., 1995, Absolute instability of the boundary layer on a rotating disk, *J. Fluid Mech.*, **229**, 17-33.

REID W. H., 1965, The stability of parallel flows. In *Basic Developments in Fluid Dynamics*, Vol. I,, Holt M. Ed., Academic Press, 249-307.

ROSS J. A., BARNES F. H., BURNES J. G., ROSS M. A. S., 1970, The flat plate boundary layer. Part 3, Comparison of theory and experiment, *J. Fluid Mech.*, **43**, 819-832.

SARIC W. S., 1990, Low-speed experiments for stability measurements. In *Instability and Transition*, Vol. I, Hussaini M. Y. and Voigt R. G. eds., Springer-Verlag, 162-174.

SEIFERT A., WYGNANSKI I. J., 1995, On turbulent spots in a laminar boundary layer subjected to a self-similar adverse pressure gradient, *J. Fluid Mech.*, **296**, 185-209.

SEIFERT A., 1996, Nonlinear evolution of point-source disturbances in an adverse pressure gradient laminar boundary layer. In *Proc. IUTAM Symp. on Nonlinear Instability and Trnnsition in Three-Dimensional Boundary Layers*, Kluwer Academic Press, 187-196.

SMITH F. T., 1979*a*, On the nonparallel flow stability of the Blasius boundary layer. *Proc. R. Soc. Lond.*, **A 366**, 91-109.

SMITH F. T., 1979*b*, Nonlinear stability of boundary layers for disturbances of various sizes, *Proc. R. Soc. Lond.*, **A 368**, 573-589.

SMITH F. T., BURGGRAF O. R., 1985, On the development of largz-sized short-scaled disturbances in boundary-layers, *Proc. R. Soc. Lond.*, **A 399**, 25-55.

WUBBEN F. J. M., PASSCHIER D. M., VAN INGEN J. L., 1990, Experimental investigation of Tollmien Schlichting instability and transmission in similar boundary layer flow in an adverse pressure gradient. In *Proc. IUTAM Symp. on Laminar-Turbulent Transition*, ARNAL D. and MICHEL R. eds., Springer-Verlag, 31-42.

(Manuscript received February 19, 1997;
revised August 15, 1997;
accepted October 29, 1997.)